frontiers | Frontiers in Earth Science

TYPE Original Research
PUBLISHED 08 February 2023
DOI 10.3389/feart.2023.1091595

OPEN ACCESS

EDITED BY
Chong Xu,
Ministry of Emergency Management, China

REVIEWED BY
Ping Wang,
China Earthquake Administration, China
Bo Zhao,
Institute of Mountain Hazards and Environment (CAS), China
Yuandong Huang,
Ministry of Emergency Management, China

*CORRESPONDENCE
Jeffrey S. Perez,
jeffrey.perez@phivolcs.dost.gov.ph

†These authors have contributed equally to this work and share first authorship

SPECIALTY SECTION
This article was submitted to Geohazards and Georisks, a section of the journal Frontiers in Earth Science

RECEIVED 07 November 2022
ACCEPTED 23 January 2023
PUBLISHED 08 February 2023

CITATION
Perez JS, Llamas DCE, Dizon MP, Buhay DJL, Legaspi CJM, Lagunsad KDB, Constantino RCC, De Leon RJB, Quimson MMY, Grutas RN, Pitapit RSD, Rocamora CGH and Pedrosa MGG (2023), Impacts and causative fault of the 2022 magnitude (M_w) 7.0 Northwestern Luzon earthquake, Philippines. *Front. Earth Sci.* 11:1091595. doi: 10.3389/feart.2023.1091595

Impacts and causative fault of the 2022 magnitude (M_w) 7.0 Northwestern Luzon earthquake, Philippines

Jeffrey S. Perez*†, Deo Carlo E. Llamas†, Margarita P. Dizon, Daniel Jose L. Buhay, Crystel Jade M. Legaspi, Kristine Dionne B. Lagunsad, Ryan Christian C. Constantino, Roland Joseph B. De Leon, Marc Marion Y. Quimson, Rhommel N. Grutas, Ron Stephen D. Pitapit, Cyrah Gale H. Rocamora and Mike Gabriel G. Pedrosa

Department of Science and Technology—Philippine Institute of Volcanology and Seismology (DOST-PHIVOLCS), Quezon City, Philippines

At 00:43 UTC on 27 July 2022, a 15-km deep major earthquake with magnitude (M_w) 7.0 struck Northwestern Luzon, Philippines. The strongest ground shaking felt was at PHIVOLCS Earthquake Intensity Scale (PEIS) VII (destructive), equivalent to Modified Mercalli Intensity (MMI) VII, in Abra and along the coastal areas of Ilocos Sur. More than a thousand landslides, rockfalls and tension cracks were mapped, near the epicentral region, in the northwestern part of the Central Cordillera. Most of the landslides were shallow-seated, many of which were situated along road cuts. Liquefaction manifested as lateral spreads, sand boils, fissures, ground subsidence, and localized swelling was documented along the coastal areas of Ilocos Sur and river channels in Abra and Ilocos Sur. Sea level disturbance was also observed in some coastal areas of Ilocos Sur and La Union. Damages to buildings and infrastructures were documented in areas that experienced PEIS VI (very strong), equivalent to MMI VI and PEIS VII (destructive). Earthquake data, including hypocentral location, aftershock distribution, focal mechanism solutions and strong motion data, and InSAR observation indicate that the earthquake was generated by an almost north-south striking reverse left-lateral oblique fault that is gently dipping to the east. There is no clear indication of a surface rupture based on InSAR analysis and field investigation. The spatial distribution of geologic impacts, such as earthquake-induced landslides and liquefaction, is strongly controlled by the causative fault, the direction of rupture propagation and geology. Peak ground acceleration (PGA) records show a unidirectional rupture propagation and are congruent with the spatial distribution of earthquake impacts. Although earthquake parameters, deformation analysis and field data suggest that the Abra River Fault is the probable causative fault, the derived geometry and kinematics from the seismotectonic analysis challenge our existing understanding of the nature of the Abra River Fault, as well as the other segments of the Philippine Fault. The need to understand these earthquake sources in the country is needed for a better seismic hazard and risk assessment.

KEYWORDS

Philippine Fault, InSAR analysis, PHIVOLCS Earthquake Intensity Scale (PEIS), liquefaction, landslide

1 Introduction

For the past 10 years, damaging earthquakes with magnitude (M_w) greater than 6 have occurred in the Philippines. These include the 2012 M_w 6.7 Negros Earthquake (PHIVOLCS, 2015; Aurelio et al., 2017; Rimando et al., 2020), the 2013 M_w 7.2 Bohol Earthquake (PHIVOLCS, 2013; Lagmay and Eco, 2014; Rimando et al., 2019), the 2017 M_w 6.5 Surigao Earthquake (PHIVOLCS QRT, 2018a), 2017 M_w 6.5 Leyte Earthquake (PHIVOLCS QRT, 2018b), the 2019 M_w 6.1 Central Luzon Earthquake (PHIVOLCS QRT, 2019), the Cotabato Earthquake Sequence (PHIVOLCS, 2019) and the 2020 M_w 6.6 Masbate Earthquake (PHIVOLCS, 2020). Detailed mapping of geologic impacts such as surface rupture, liquefaction, earthquake-induced landslides and tsunamis was conducted together with social-economic impacts. Reports generated from these earthquakes were used by different stakeholders for the assessment of hazards and identification and characterization of the causative faults.

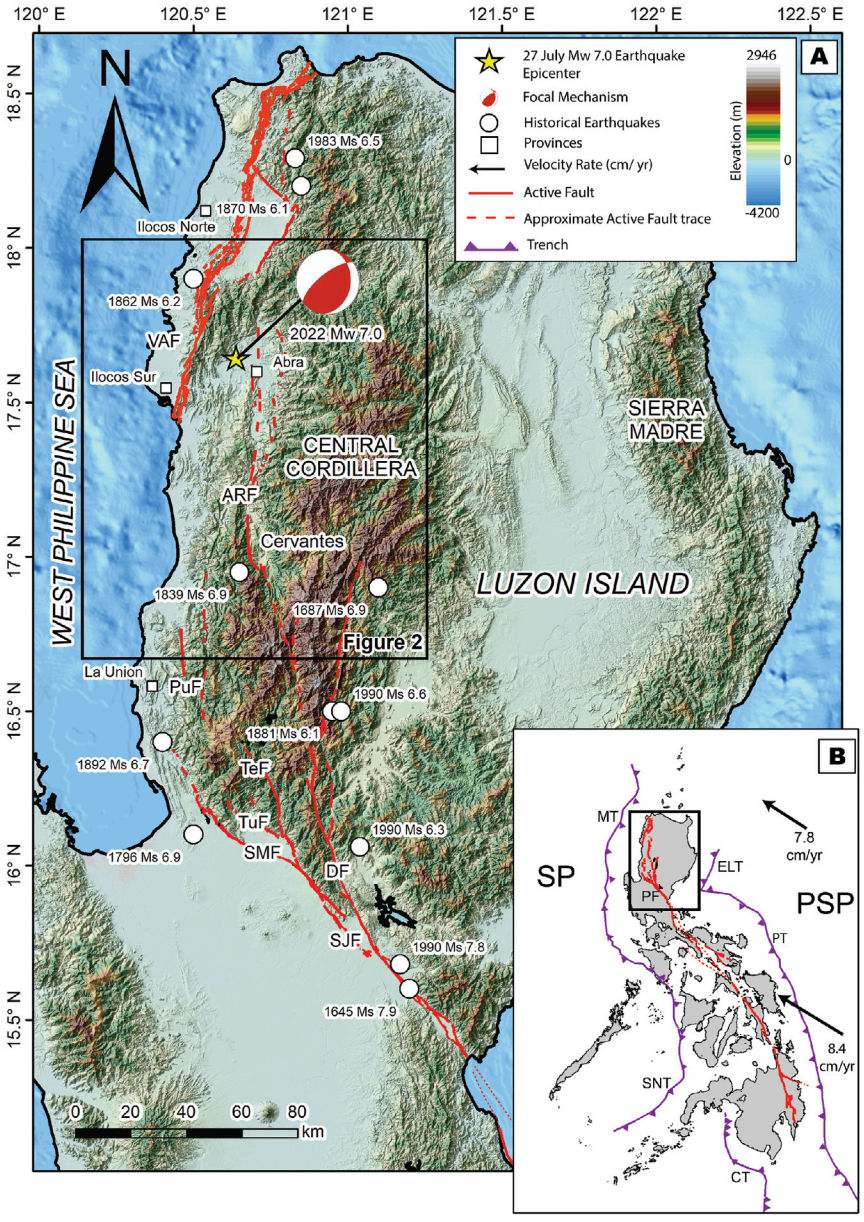

FIGURE 1
The tectonic setting of the 2022 Mw 7.0 Northwestern Luzon Earthquake. **(A)** The northern branch Philippine Fault and its associated significant earthquakes in Northern Luzon from 1700 to 2022 (other active faults are not shown). SJF—San Jose Fault, DF—Digdig Fault, SMF—San Manuel Fault, TuF—Tuba Fault, TeF—Tebbo Fault, PuF—Pugo Fault, VAF—Vigan-Aggao Fault (also known as West Ilocos Fault System), ARF—Abra River Fault. **(B)** Geodynamic setting of the Philippines. The Philippines is a complex boundary between the obliquely converging Philippine Sea Plate and the Sunda Plate. Arrows indicate the motion velocity of the Philippine Sea Plate (Zang et al., 2002). SP—Sundaland Plate, PSP—Philippine Sea Plate, MT—Manila Trench, ELT—East Luzon Trough, PT—Philippine Trench, SNT—Sulu-Negros Trench, CT—Cotabato Trench, PF—Philippine Fault. The Philippine Fault and the location of trenches are from Tsutsumi and Perez (2013) and PHIVOLCS (2022a) while the epicenters are from SEASSE (1985) and Bautista and Oike (2000). Basemap is from the Philippine National Mapping and Resource Information Authority (NAMRIA) and the General Bathymetric Chart of the Oceans (GEBCO). The rectangle in **(A)** shows the location of Figure 2.

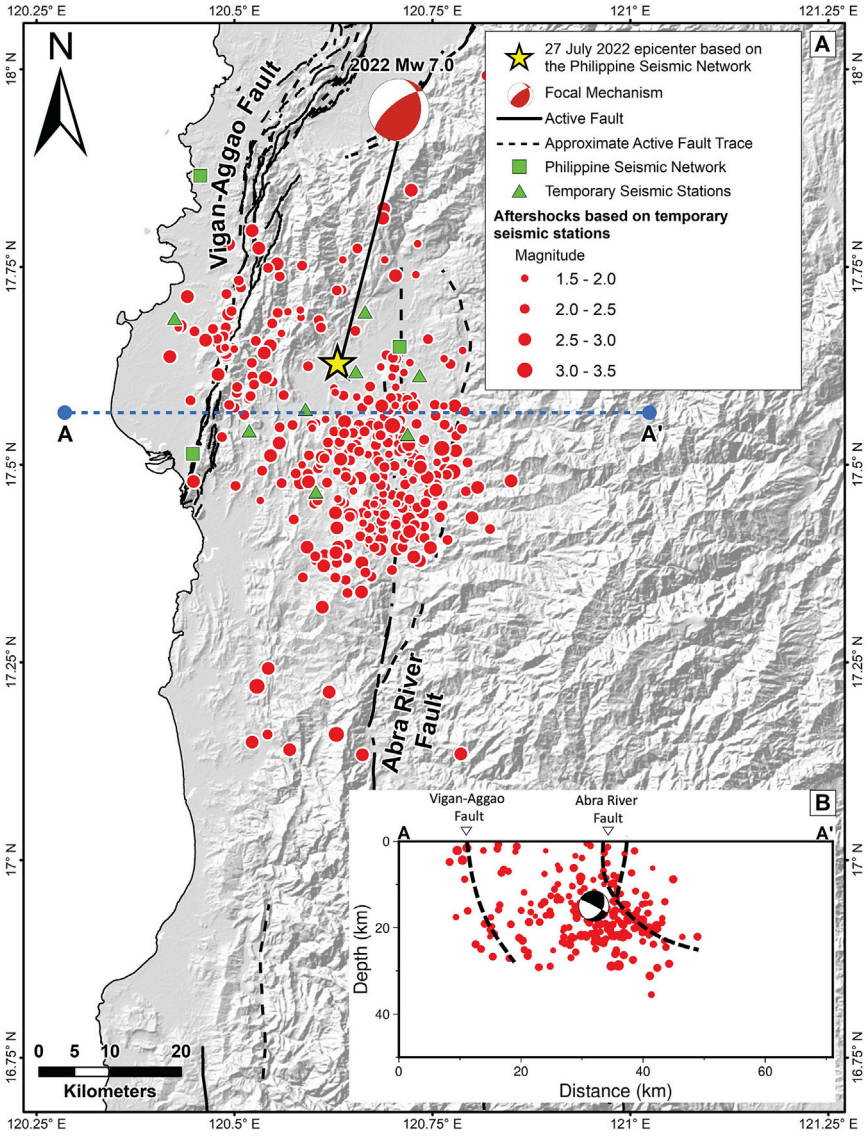

FIGURE 2
Aftershocks after the 27 July Mw 7.0 Northwestern Luzon Earthquake. **(A)** Aftershock distribution from 28 to 30 July 2022 was recorded by the temporary seismic stations installed around the epicentral region. **(B)** East-west cross-section of the aftershock distribution. From the spatial distribution of aftershocks, we can observe two clusters of aftershocks, first along the Abra River Fault and second, along the southern portion of the Vigan-Aggao Fault.

On 27 July 2022 at 00:43 UTC (8:43 a.m., local time), another M_w 7.0 damaging earthquake occurred in northwestern Luzon Island, Philippines (Figure 1A). The Philippine Seismic Network (PSN) located the earthquake's hypocenter at 3 km N50W of Tayum, Abra (17.63 N, 120.63 E) with a depth of 15 km. As of 05 September 2022, the PSN recorded a total of 5,573 aftershocks of which 77 are felt events with magnitudes ranging from 1.4 to 5.2.

This earthquake has greatly affected two provinces in the northern Philippines—Abra and Ilocos Sur—and generated earthquake-induced landslides, liquefaction and sea level disturbances. Strong shaking was felt with a maximum felt intensity of PHIVOLCS Earthquake Intensity Scale (PEIS) VII (destructive) which is equivalent to Modified Mercalli Intensity (MMI) VII and caused damage to properties and infrastructures worth approximately 46 million US dollars. This earthquake was the first magnitude 7 earthquake along the Philippine Fault after the 1990 M_w 7.7 Luzon Earthquake more than 30 years ago. The 1990 Luzon Earthquake was considered to be the most damaging earthquake in the country with damage to properties worth more than 0.5 billion US dollars and was also generated by one of the segments of the Philippine Fault (Nakata et al., 1996).

To immediately assess the impacts of the earthquake, the Department of Science and Technology - Philippine Institute of Volcanology and Seismology (DOST-PHIVOLCS) immediately deployed a Quick Response Team (DOST-PHIVOLCS QRT) less than 12 hours after the earthquake. The DOST-PHIVOLCS QRT is composed of geologists, engineers, and social scientists and was sent to the affected areas to document and map the effects of the earthquake from 27 July 2022 to 07 August 2022. On 28 July, an aerial survey was conducted to immediately assess the possible extent of geologic and structural

impacts. After this, field investigation followed which includes describing and locating the geologic impacts using handheld GPS and remotely piloted aircraft (RPA), eyewitness interviews and photo documentation. Eight temporary seismic stations were also installed by the DOST-PHIVOLCS QRT around the epicentral area for aftershock monitoring (Figure 2A). An additional inventory of landslides triggered by the earthquake was generated using high-resolution, pre- and post-earthquake satellite images. In this paper, we present the results of the field investigation, assessment and documentation of the geologic and socio-economic impacts of the 2022 M_w 7.0 Northwestern Luzon Earthquake. We provide an initial interpretation of the causative fault using earthquake and InSAR data and our field observation. We also discuss the characteristics of this segment of the Philippine Fault and in general, its relation to the seismic hazard in the Philippines.

2 Tectonic setting

Luzon Island, the largest island in the Philippine archipelago, is traversed by the Philippine Fault, a ~1,500-km-long left-lateral strike-slip fault, and cuts the entire archipelago from Luzon Island on the north to eastern Mindanao on the south (Figure 1B) (Tsutsumi and Perez, 2013). This fault accommodates the trench-parallel component of the oblique convergence of the Sunda Plate and the northwestward drifting Philippine Sea Plate (Fitch, 1972). An average slip rate of 2–3 cm/yr was computed by Barrier et al. (1991) from earthquake slip vectors and regional kinematic data for the Philippine Fault. This estimation was supported by various geodetic and GPS measurements (Duquesnoy et al., 1994; Aurelio, 2000; Galgana et al., 2007) (Figure 1B). Paleoseismic information along the different segments of the Philippine Fault also revealed recurrence intervals of less than 1000 years (Daligdig, 1997; Tsutsumi et al., 2006; Papiona and Kinugasa, 2008; Perez et al., 2015; Tsutsumi et al., 2015; Perez and Tsutsumi, 2017).

In northern Luzon, the Philippine Fault bifurcates into several branches bounding or cutting through the Central Cordillera (Figure 1A). Among its branches are the Digdig Fault, the San Jose Fault, the San Manuel Fault, the Pugo Fault, the Tebbo Fault, the Tuba Fault, the Abra River Fault, and the Vigan-Aggao Fault (also known as West Ilocos Fault System) (Pinet and Stephan, 1990; Ringenbach et al., 1993; Rimando and Knuepfer, 2006; Tsutsumi and Perez, 2013; Rimando and Rimando, 2020; PHIVOLCS, 2022a) (Figure 1A). The Central Cordillera is a north-south trending mountain range composed of deformed and metamorphosed basement rocks cut by a series of intrusive and extrusive rocks and overlain by shallow to deep marine sedimentary rocks (Pinet and Stephan, 1990; Yumul et al., 2008). The northern branches of the Philippine Fault are characterized as a braided strike-slip system (Pinet and Stephan, 1990) with a significant thrust component (Barrier et al., 1991; Nakata et al., 1996; Pinet and Stephan, 1990; Ringenbach et al., 1990).

Abra, the epicentral area, is located in the northwestern part of the Central Cordillera. It is traversed by the Abra River Fault (ARF) and bounded to the west by the Vigan-Aggao Fault (VAF) (Figure 1A). The Abra River Fault is a left lateral strike-slip fault that acts as the central branch of the Philippine fault in the Cordillera (Ringenbach et al., 1990). The fault forms a releasing bend in the Cervantes area and then continues northward with an approximately N-S trending strike. It is characterized by wide deformation zones with almost vertical tectonic gouges measuring over 100 m in width. Fault strands indicating a thrust component were also observed by Ringenbach et al. (1990) near the southern portion of the fault raising sedimentary and basement rocks westward. On the other hand, the Vigan-Aggao Fault is the westernmost splay of the Philippine Fault in northern Luzon with dominant sinistral strike-slip movement as evidenced from horizontal and vertical measurements (Rimando and Rimando, 2020).

For the past 450 years, with written Philippine historical earthquake documents and/or seismic instrumentation, at least two magnitude >6 earthquakes can be attributed along the Abra River Fault (Figure 1A). The 1839 magnitude 6.9 earthquake occurred 75 km south of the epicenter of the 2022 M_w 7.0 earthquake while the epicenter of the 1870 magnitude 6.1 earthquake was located 65 km north of Abra (SEASEE, 1985; Bautista and Oike, 2000; PHIVOLCS, 2020b). These two earthquakes caused severe ground shaking and damage to structures in the provinces of Ilocos Sur and Ilocos Norte (SEASEE, 1985). Other magnitude >6 earthquakes in the region were generated by the different segments of the Philippine Fault (Figure 1A).

3 Earthquake source fault

3.1 Aftershock distribution

To augment the PSN and to constrain the spatial distribution of the aftershocks of the 2022 Northwestern Luzon Earthquake, eight additional temporary seismic stations were installed by the DOST-PHIVOLCS QRT around the epicentral region. Figure 2A shows the aftershock distribution for 3 days (28–30 July 2022) while Figure 2B is an east-west cross-section. The aftershock distribution appears to have a northerly trend and favors a N-S striking fault plane that is gently dipping to the east consistent with the derived focal mechanism (Section 3.2; Figure 1A, Figure 3). We can also observe two clusters of aftershocks, most of the aftershocks were located along the Abra River Fault while the second cluster was along the southern portion of the Vigan-Aggao Fault (Figure 2).

3.2 Focal mechanism

Using the PSN, DOST-PHIVOLCS adapted the Source parameter determination based on Waveform Inversion of Fourier Transformed seismograms (SWIFT) to determine the centroid moment tensor (SWIFT-CMT) of the earthquake. This method conducts a waveform inversion in the frequency domain of body waves from broadband seismic stations in the Philippines for more efficient calculation (Nakano et al., 2008; Bonita et al., 2015; Punongbayan et al., 2015). Calculated SWIFT-CMT solution for this earthquake indicates that the faulting occurred on either a N-S striking, east-dipping nodal plane with a strike of 8°, a dip of 28°, and a rake of 49°, or a NE-SW striking, NW-dipping nodal plane with a strike of 233°, a dip of 69° and a rake of 109° (Figure 1A, Figure 2A) (PHIVOLCS, 2022e). A seismic moment (Mo) of 4.01×10^{19} N.m. and M_w of 7.0 was obtained from the inversion. The focal mechanism derived from the SWIFT-CMT solution shows a significant reverse slip component and is also comparable to the focal mechanism solutions presented by different seismological institutions such as US Geological Survey (USGS, 2022), Geofon (Geoscope Observatory, 2022), GCMT (Dziewonski et al., 1981; Ekström et al., 2012; Global Centroid

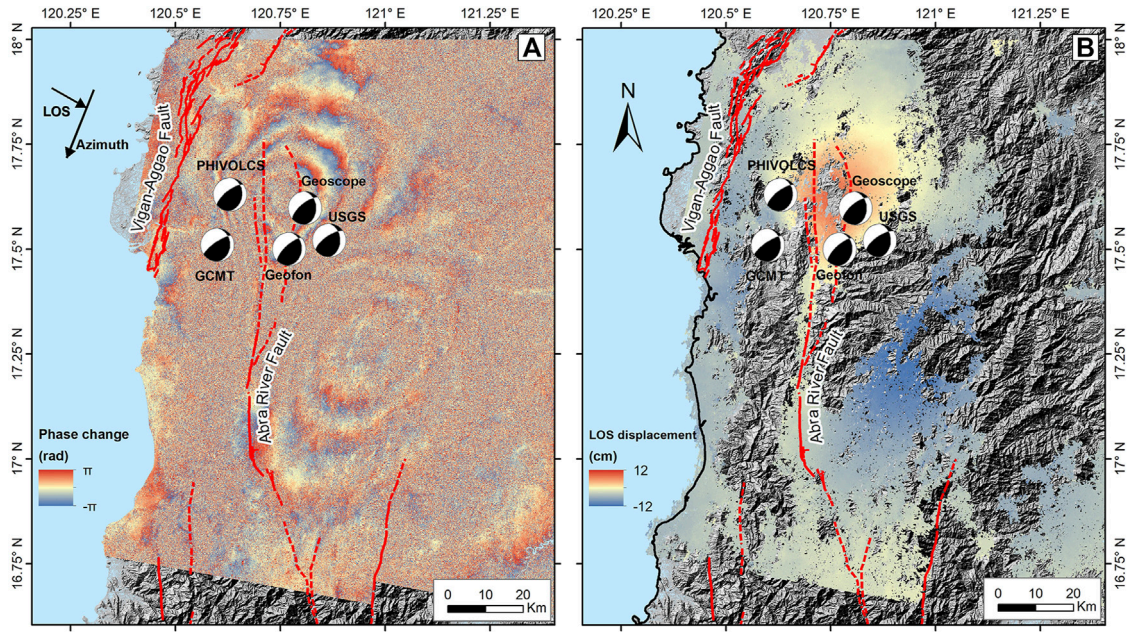

FIGURE 3
Coseismic deformation observed from InSAR using Sentinel-1 images (06/27/2022 and 08/02/2022) descending track. **(A)** Interferogram shows coseismic deformation concentrated at the eastern side of the Abra River Fault; one cycle of fringes is equivalent to 2.8 cm. **(B)** Unwrapped LOS displacement field indicates movement toward the satellite (red areas) on the northern portion, while movement away from the satellite (blue areas) on the southern portion. Areas with low coherence were masked. Focal mechanism solutions were from DOST-PHIVOLCS, USGS, GCMT, Geofon and Geoscope.

Moment Tensor, 2022), and Geoscope (GFZ German Research Center for Geosciences, 2022) (Figure 3).

3.3 InSAR observation

To constrain the coseismic deformation associated with the 2022 M_w 7.0 Northwestern Luzon Earthquake, we conducted differential Interferometric Synthetic Aperture Radars (InSAR) analysis and used the SAR images from the descending track of Sentinel-1A provided by the European Space Agency (ESA). We applied a typical two-pass approach to process the pre- and post-earthquake images (27 June 2022 and 02 August 2022) using the InSAR Scientific Computing Environment version 2 (ISCE2) software (Rosen et al., 2012).

Despite the fact that many areas display low coherence probably due to dense vegetation, the coseismic interferogram (Figure 3A) reveals clear concentrations of interferometric fringes that seem to form a north-south deformation pattern. The northern fringes indicate movement toward the satellite while the southern fringes suggest a movement away from the satellite. Peak displacements reach 14 cm in the radar line-of-sight (LOS) direction, based on the displacements derived from the unwrapped interferogram (Figure 3B). A primary surface rupture, however, was not evident in the interferograms. Moreover, the deformation is mostly concentrated on the eastern block of the Abra River Fault. This is similar to the deformation pattern of faults with significant reverse motion in which deformation generally appears on the hanging wall (Donahue and Abrahamson, 2014; Abrahamson and Silva, 1997; Chang et al., 2005; Su et al., 2019).

4 Earthquake impacts

4.1 Ground shaking intensities and isoseismal map

The earthquake shook almost the entire Luzon Island, including Metro Manila, the capital of the Philippines, and as far as 500 km south of the epicenter (Camarines Norte). Based on the latest earthquake information (PHIVOLCS, 2022c) and the result of the DOST-PHIVOLCS QRT field investigation and impact assessment, we have summarized the observed earthquake impacts and earthquake intensity and generated an isoseismal map for this event (Figure 4). The isoseismal map is based on the PEIS, a 10-point earthquake intensity scale used in the Philippines (PHIVOLCS, 2022d) with PEIS X (completely devastating) as the maximum, which is comparable with the MMI scale.

The maximum earthquake intensity for this event was PEIS VII (destructive) equivalent to MMI VII and was felt mostly in Abra and the coastal areas of Ilocos Sur (Figure 4). The maximum intensity was felt for about 2,200 sq. km. Areas with PEIS VII (destructive) suffered significant damage to old and poorly built structures while some well-built structures, mostly residential houses, are slightly damaged. Based on interviews by the DOST-PHIVOLCS QRT, people in these areas were frightened and some ran outdoors. Liquefaction, landslides and sea level disturbance were also documented in these areas (Figures 5–9). The rest of Ilocos Sur, parts of Ilocos Norte, La Union, Mountain Province and Kalinga felt the earthquake at PEIS VI (very strong) equivalent to MMI VI. People in these areas were frightened and some run outdoors. They observed cracks in wall plaster and significant

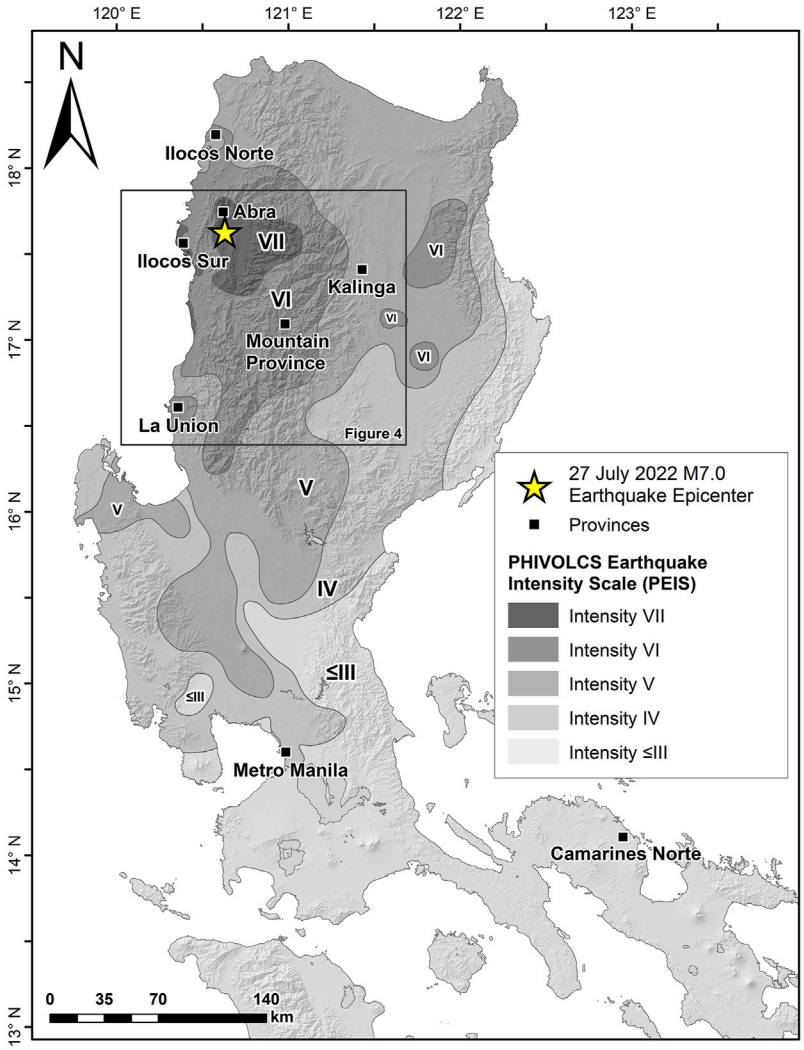

FIGURE 4
The 27 July M7.0 Northwestern Luzon Earthquake Isoseismal Map. The isoseismal map was based on the latest earthquake information (PHIVOLCS, 2022c) and the result of the DOST-PHIVOLCS QRT field investigation and impact assessment. The intensities used for the isoseismal map are based on the PHIVOLCS Earthquake Intensity Scale (PEIS) (PHIVOLCS, 2022d). The rectangle shows the location of Figure 5.

damage to old and poorly constructed structures. Rockfalls were also documented in these areas. Detailed descriptions of the earthquake impacts will be discussed in the next sections.

The peak ground acceleration (PGA) values of the M_w 7.0 Northwestern Luzon Earthquake recorded by the Philippine Strong Motion Network (PSMNet) of DOST-PHIVOLCS in Ilocos Norte, Ilocos Sur and La Union show that the highest PGA value, 0.29 g, was recorded by the ISCC station in Ilocos Sur, ~55 km southwest of the epicenter (Figure 5 and Table 1). Other stations in Ilocos Sur and La Union have recorded PGA values ranging from 0.11 to 0.26 g and 0.09–0.14 g respectively (Table 1). Although the ISSD station is closer to the epicenter, it has recorded a relatively lower PGA value of 0.19 g compared to the stations in the central part of Ilocos Sur (ISNR: 0.26 g; ISSE: 0.23 g; and ISCC: 0.29 g). It can be observed that the actual PGA values recorded by stations in Ilocos Sur generally increase from north to south (Figure 5). We have also observed that the PGA values for this event also correspond to the assessed intensity in Ilocos Sur, Ilocos Norte and La Union.

4.2 Surface rupture

Guided by the previously mapped and identified active faults in the area (Figures 1A, 2A) and differential InSAR results (Figure 3), the DOST-PHIVOLCS QRT visited areas that were suspected to have a fault rupture. Moreover, pre-existing maps were complemented by quick morphotectonic analysis for possible unmapped active faults in the area. Reports of fissures and cracks were assessed based on the following criteria such as 1) lateral continuity, 2) consistent strike, 3) offsets consistent with the expected fault mechanism, 4) structural characteristics and 5) association with pre-existing morphology. No surface rupture related to the movement of the Abra River Fault and the 2022 M_w 7.0 Northwestern Luzon Earthquake was identified

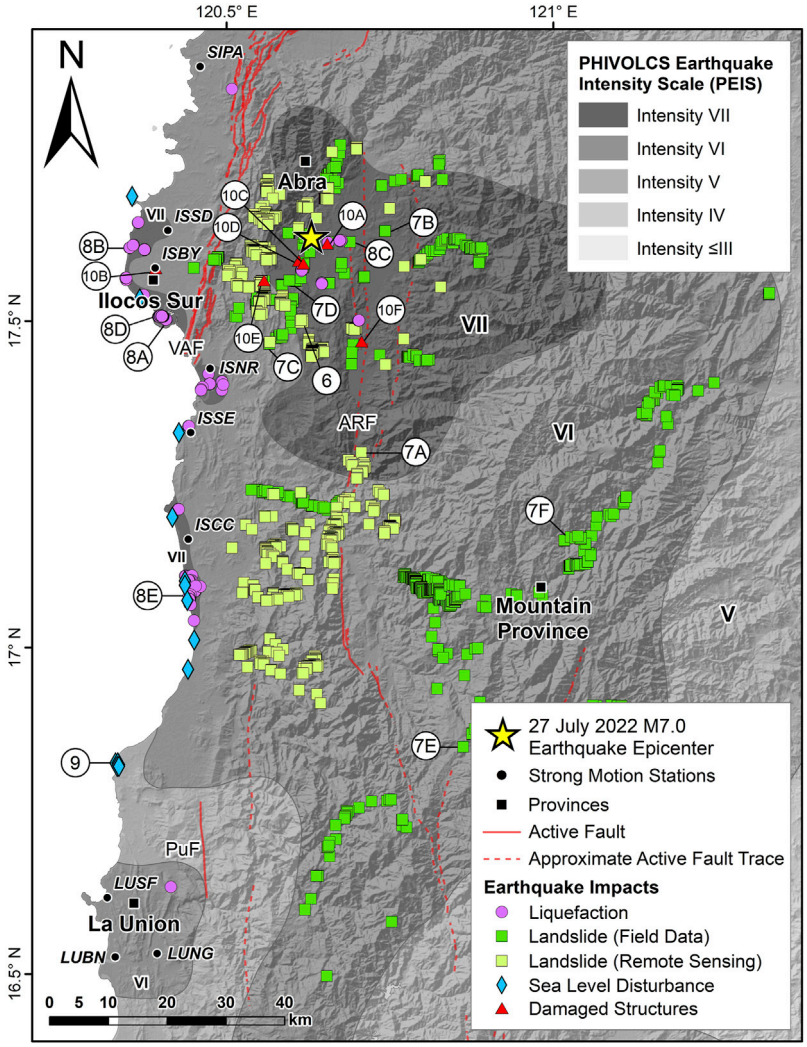

FIGURE 5
Impact Map of the 2022 M7.0 Northwestern Luzon Earthquake. Spatial distribution of documented geologic impacts, (earthquake-induced landslides, liquefaction and sea level disturbance) during the 2022 Mw 7.0 Northwestern Luzon Earthquake. Black circles show the location of the accelerographs with station code from the Philippine Strong Motion Network (PSMNet). Circles with letters and numbers show the location of photos in Figures 6–10. PuF—Pugo Fault, VAF—Vigan-Aggao Fault (also known as West Ilocos Fault System), ARF—Abra River Fault.

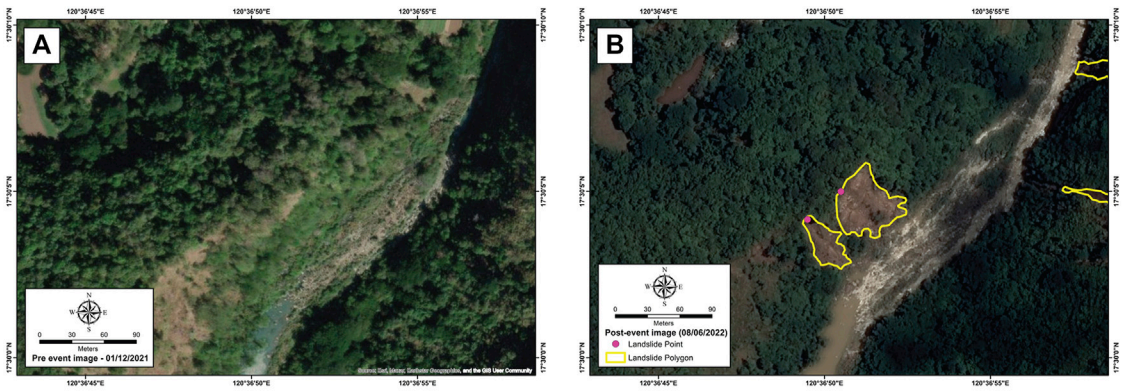

FIGURE 6
Comparison of remote sensing images for landslide identification. **(A)** Pre-event satellite image taken on 12 January 2021 (Source: Esri, Maxar, Earthstar Geographics and the GIS User Community); **(B)** Landslides (yellow polygon) identified using post-event satellite image taken on 06 August 2022 (Source: Pleiades 1B). Refer to Figure 5 for the location of the landslide.

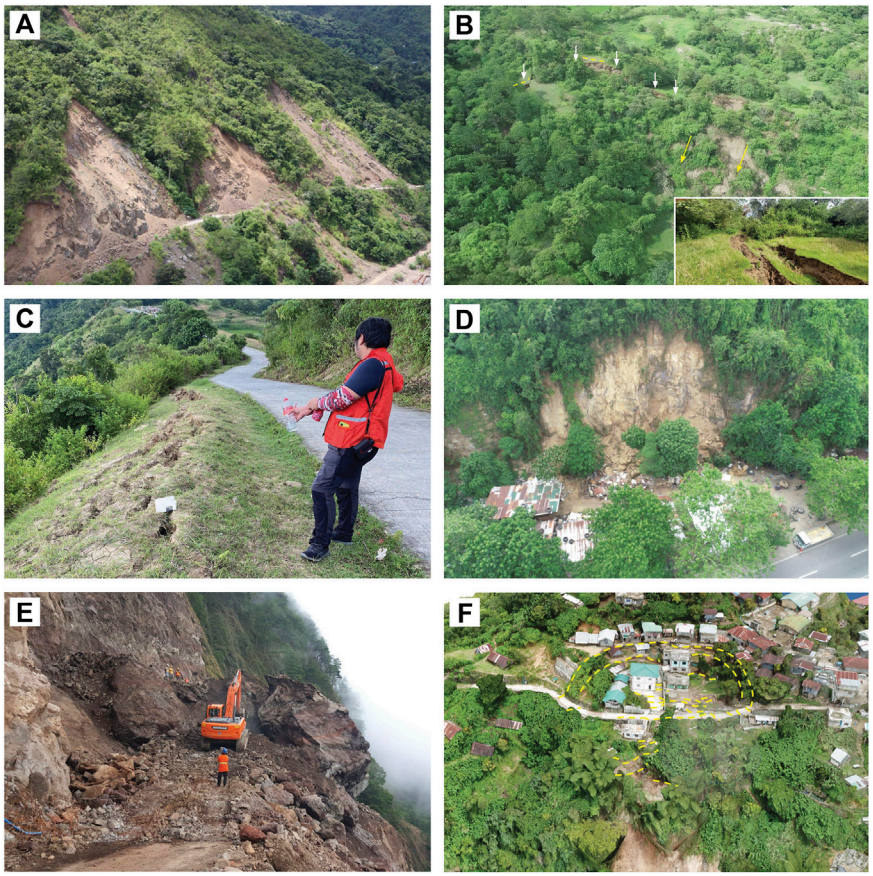

FIGURE 7
Documented landslides after the 2022 Mw 7.0 Northwestern Luzon Earthquake. **(A)** Aerial photo of series of roadcut landslides which caused road blockages in Luba, Abra; **(B)** Drone imagery of the tension cracks (white arrow) and landslides (yellow arrows) in Dolores, Abra; **(C)** Series of tension cracks traverse the ridge crest in along the boundaries of San Isidro, Abra and Nagbukel, Ilocos Sur; **(D)** Aerial photo of the observed rockslide on a steep slope adjacent to several residential houses Bangued, Abra; **(E)** Massive rockslide along the Benguet-Mt. Province National Road in Bauko, Mt. Province. **(F)** Aerial photo of the deep-seated rotational slide with landslide crown near residential houses associated with a series of tension cracks and roadslip progressing downslope in Sadanga, Mt. Province. Refer to Figure 5 for the location of the photographs.

during our field investigation and the observed tension cracks were related to landslides or fissures related to liquefaction.

4.3 Earthquake-induced landslides

More than a thousand earthquake-induced landslides were identified in the mountainous regions of Abra, Mountain Province, Ilocos Sur and La Union in the northwestern portion of the Central Cordillera after the earthquake (Figure 5). Out of the 1,474 landslides mapped, 823 were documented during the DOST-PHIVOLCS QRT field investigation while the remaining 651 landslides were identified from the inventory using post-event images taken by the Pleiades and Worldview 2 satellites (Figure 6 and Supplementary Table S1). Mapped landslides for this event are located in areas with metamorphosed basement rocks, series of intrusive and extrusive igneous rocks and shallow to deep marine sedimentary rocks (Pinet and Stephan, 1990; MGB, 2008). Landslides were identified as far as 125 km south of the epicenter.

These landslides were manifested as shallow-translational slides, rockslides, and some deep-rotational slides which caused damage to buildings and infrastructures, road blockage, isolation of communities, temporary community evacuation, and casualties. Translational slides and rockslides commonly occurred adjacent to road cuts that lacked proper slope protection and reinforcement (Figure 7A). Tension cracks and deep-rotational slides, in contrast, were documented more commonly on hillslopes (Figure 7B). Some notable earthquake-induced landslides observed are extensive tension cracks with some failures observed near the boundaries of San Isidro, Abra and Nagbukel, Ilocos Sur (Figure 7C); rockslides near the residential houses in Bangued, Abra (Figure 7D) that resulted to the immediate evacuation of the community; road blockage caused by rockslides and landslides, an example is a massive rockslide in Bauko, Mountain Province (Figure 7E); and a deep-seated rotational landslide with identified landslide crown associated with a series of tension cracks and road displacement in Sadanga, Mountain Province (Figure 7F). Areas with landslides were assigned to PEIS VI (very strong) and PEIS VII (destructive) (Figures 4, 5).

4.4 Liquefaction

In both Abra and Ilocos Sur, liquefaction occurred in several lowlands characterized by unconsolidated recent deposits and

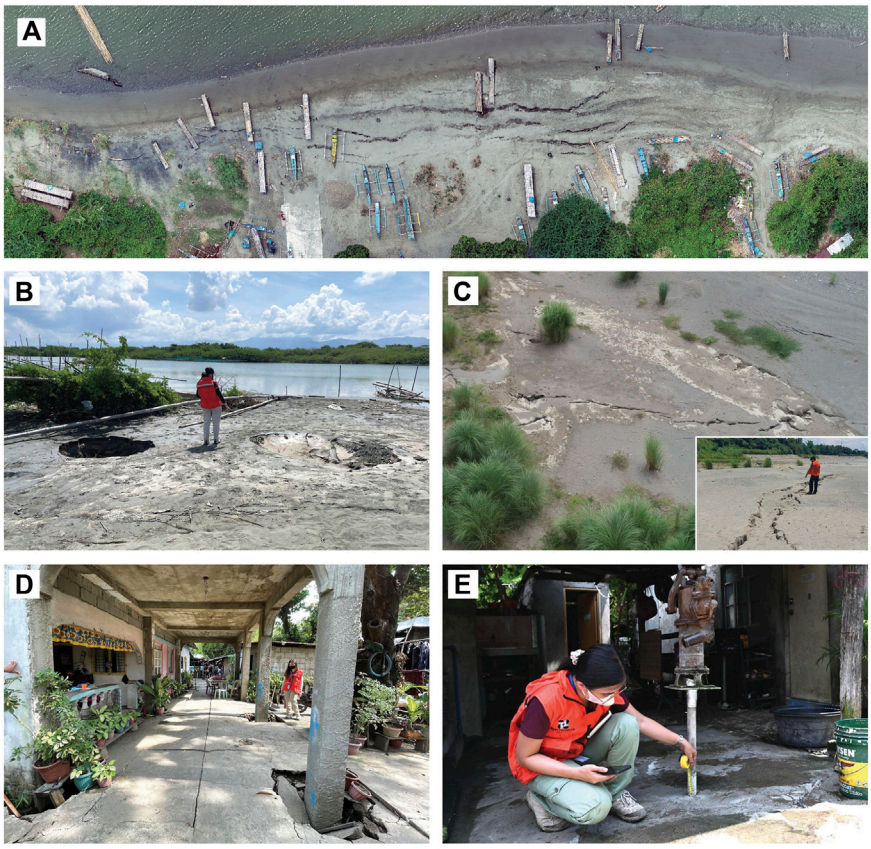

FIGURE 8
Documented liquefaction after the 2022 Mw 7.0 Northwestern Luzon Earthquake. **(A)** An orthophoto (derived using remotely piloted aircraft) of lateral spreads along the coast of Santa, Ilocos Sur which extends to approximately 300 m; **(B)** Numerous sand boils on the coast of San Vicente in Ilocos Sur; **(C)** Ground fissures along a point bar of the Abra River in Tayum, Abra; **(D)** Building settlement of approximately 45 cm on a delta in Caoayan, Ilocos Sur; **(E)** Raised artesian well with 10 cm displacement in Santa Cruz, Ilocos Sur. Refer to Figure 5 for the location of the photographs.

TABLE 1 Peak ground accelerations from the Philippine Strong Motion Network (PSMNet). Refer to Figure 4 for the location of the stations.

Strong motion station code	Measured peak ground acceleration g)	Distance from the epicenter (km)
SIPA	0.11	34 km northwest
ISSD	0.19	23 km west
ISBY	0.13	26 km west
ISNR	0.26	29 km southwest
ISSE	0.23	39 km southwest
ISCC	0.29	55 km southwest
LUSF	0.09	117 km southwest
LUNG	0.11	124 km southwest
LUBN	0.14	126 km southwest

sediments and shallow groundwater (MGB, 2008) (Figure 5, Figures 8A–E). Some of the liquefaction impacts appeared along the flood plains, tributaries and point bars of the Abra River, which meanders through the western portion of Abra and drains towards its delta located west of Ilocos Sur. Liquefaction was also documented on beaches, fills, marshes, and other river banks facing the West Philippine Sea and as far as 110 km southwest from the epicenter.

The DOST-PHIVOLCS QRT has mapped more than 300 areas affected by liquefaction (Supplementary Table S1). These were documented during the field investigation and using remotely piloted aircraft (RPA) (Figures 8A–E). Ground failures associated with liquefaction include lateral spreads (Figure 8A), sand boils (Figure 8B), ground fissures (Figure 8C), ground subsidence, and localized ground swelling. Aside from ground failures,

FIGURE 9
Documented sea level disturbance after the 2022 Mw 7.0 Northwestern Luzon Earthquake. **(A)** Interviews were conducted in the field to verify the reports of sea level disturbance after the earthquake. Interviewees reported a 2-m-high wave in Luna, La Union; **(B)** onshore extent (person standing) of displaced boats docked along the coast. Refer to Figure 5 for the location of sites with reports of sea level disturbance.

liquefaction also caused damage to built-up areas. Differential settlement of buildings (Figure 8D) and uplift of buoyant structures (Figure 8E) were also documented. While liquefaction affected some large swaths of land, there were few documented structural damages since most of the liquefaction impacts occurred far from communities and developed areas. Areas with manifestations of liquefaction were assigned to PEIS VII (destructive) and most of these are located south of the epicenter (Figures 4, 5).

4.5 Sea-level disturbance

Sea level disturbance was observed in coastal areas of Ilocos Sur and La Union (Figure 5 and Supplementary Table S1). In Ilocos Sur, based on the DOST-PHIVOLCS QRT interview, residents reported a sudden drop in the sea level, which returned to normal a few seconds to minutes after the shaking. Despite the distance from the epicenter (~80 km away), 2 m high waves were noted in Luna, La Union, which displaced several boats docked along the coast (Figure 9). The observed sea level disturbance can be attributed to submarine landslides triggered by the earthquake and/or water oscillation generated by strong shaking. Detailed studies are ongoing such as bathymetric mapping and tsunami modeling and simulation to better explain this phenomenon.

4.6 Structural damage and socio-economic impacts

The DOST-PHIVOLCS QRT conducted an assessment of selected damaged structures in Abra and Ilocos Sur (Figure 5 and Figure 10A–E). Most of the surveyed buildings in Ilocos Sur are historical buildings (more than 100 years old) and were classified as unreinforced structures while in Abra, old and newly constructed structures, classified as unreinforced, reinforced and concrete hollow block (CHB) structures were assessed. In Abra, the 19th-century baroque church, Santa Catalina Alexandria Church or Tayum Church (Figure 10A), was totally damaged showing widespread large vertical, diagonal, and crisscrossing cracks in the masonry walls and its façade. The displaced large masonry wedge inside the church suggests that the structural support has been compromised. Spalling of concrete on the strengthened bell tower was also observed. The St. Augustine Church belfry built in 1591 (also known as the Bantay Bell Tower), in Ilocos Sur, experienced spalling on its façade and large cracks along the tower (Figure 10B).

It was documented by the DOST-PHIVOLCS QRT that different reinforced concrete and CHB buildings in Abra suffered different types of damages. Because of substandard columns, some multi-story residential and commercial buildings suffered pancake-type collapse (Figure 10C). Poor construction practices and substandard building design resulted in the tilting of a three-story commercial building in Abra (Figure 10D). Most of the residential houses in Abra are made up of CHB and non-engineered. Poor qualities of the CHB and steel bars have resulted in the collapse of walls and gable walls (Figure 10E). Even newly constructed multi-story, reinforced concrete buildings, some of which are government buildings, such as schools have suffered significant damages which resulted in the abandonment of these buildings (Figure 10F). Poor construction, improper building designs and substandard construction materials subjected to intense ground shaking resulted to severe damages to these reinforced concrete and CHB buildings. The buckling of roads in different areas was also documented.

Based on National Disaster Risk Reduction Management Council (NDRRMC) Situational Report No. 20, dated 22 August 2022 this earthquake affected more than 574,000 persons, claiming eight persons dead and 609 persons injured (NDRRMC, 2022). More than 36,000 residential houses and 2,700 buildings that include old historical churches were damaged. The estimated cost of damage to structures is about 2.6 billion Philippine pesos or 46 million US dollars (NDRRMC, 2022).

5 Discussion

Analysis of the earthquake parameters that include the hypocenter, aftershock distribution and focal mechanism, together with InSAR and field data suggests that the Abra River Fault is the probable causative fault of the 2022 M_w 7.0 Northwestern Luzon Earthquake. Although there is no clear indication of a surface rupture based on InSAR and field observations, the aftershock distribution (Figure 2) and the deformation pattern (Figure 3) appear to be constrained by the Abra River Fault. This north-south deformation pattern observed

FIGURE 10
Damaged structures after the 2022 Mw 7.0 Northwestern Luzon Earthquake. **(A)** Totally damaged 19th-century baroque church, the Santa Catalina Alexandria Church, in Tayum, Abra; **(B)** Damaged 16th-century belfry of the St. Augustine Church (Bantay Bell Tower); **(C)** Pancake-type collapse of a two-story residential building; **(D)** Tilted three-story commercial building; **(E)** Completely damaged concrete hollow block residential house; **(F)** Completely damaged two-story school building. Refer to Figure 5 for the location of the photographs.

from InSAR together with the clustering of aftershocks favors the north-striking and east-dipping fault plane with a reverse left-lateral oblique mechanism derived from the SWIFT-CMT solution. The strike orientation would be consistent with the tectonic context as faulting in the region involves generally the north-striking, left-lateral splays of the Philippine Fault (Pinet and Stephan, 1990; Ringenbach et al., 1993; Rimando and Knuepfer, 2006; Rimando and Rimando, 2020). However, the gentle dip and the oblique slip are not consistent with the known characteristic of the Abra River Fault. We interpret that the causative fault is a part of the positive flower structure at a depth that connects to the surface trace of the Abra River Fault (steepening upward)—which can explain the gentle dip and oblique slip of the preferred fault plane at depth (Figure 11). Surface deformation is concentrated on the east side of the Abra River Fault (which is the hanging wall), indicating typical characteristics of thrust motion as this earthquake has a significant amount of reverse slip component (Su et al., 2019) (Figure 3). The transpressive nature of the fault contributes to the continuous uplift of the Central Cordillera. Rimando et al. (2022) have suggested a possible source fault for this event using inverse modeling of InSAR observations. Their preferred fault model is an east-dipping plane in which the top of the ruptured plane is located beneath the trace of the Abra River Fault. Their ruptured fault plane model, would be consistent with our interpretation, except that their preferred surface fault projection is located west of the Abra River Fault. Further analysis using geodetic inversion and hypocentral relocation can further constrain the causative fault.

The spatial distribution of the geologic impacts may also reveal the characteristics of the causative fault. Earthquake-induced landslides are usually concentrated near the causative fault, hence their spatial distribution is generally controlled by the fault. Most of the landslides triggered by this earthquake occurred within 20 km from both sides of the causative fault, which further supports the interpretation that the Abra River Fault is the probable causative fault. Commonly, more landslides occurred on the hanging wall as compared to the footwall called the hanging wall effect (Abrahamson and Silva, 1997; Chang et al., 2005; Donahue and Abrahamson, 2014; Xu et al., 2014). However, for this earthquake, the landslides on the footwall were more than that on the hanging wall. This can be attributed to two factors. The difference in the geology of the opposite sides of the Abra River Fault may have contributed to the spatial distribution of earthquake-induced landslides (Gorum, 2013). The hanging wall is composed of metamorphosed basement rocks and a series of intrusive and extrusive igneous rocks while the footwall is overlain by shallow to deep marine

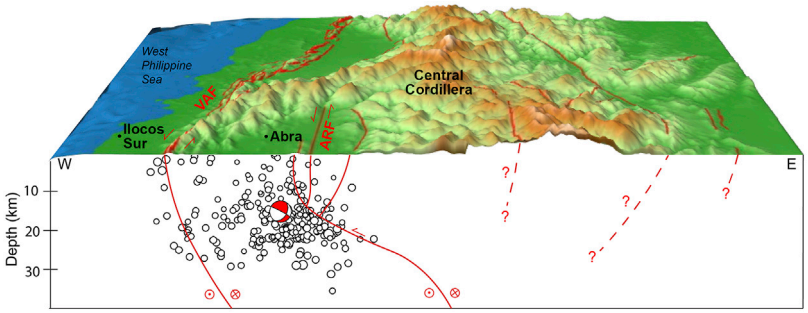

FIGURE 11
Schematic diagram of the causative fault of the 2022 Mw 7.0 Northwestern Luzon Earthquake. Sub-surface representation of the Abra River Fault (ARF), Vigan-Aggao Fault (VAF) (also known as West Ilocos Fault System) and other faults in the region based on focal mechanism solution and clustering of aftershocks. The causative fault, which has a gentle dip and oblique-slip is a part of the positive flower structures at a depth that connects to the surface trace of the Abra River Fault. Open black circles are aftershocks after the 2022 Mw 7.0 Northwestern Luzon Earthquake (Section 3.1). The focal mechanism solution is from DOST-PHIVOLCS SWIFT-CMT Solution (Section 3.2). Red lines are traces of active faults.

sedimentary rocks (Pinet and Stephan, 1990; MGB, 2008). Another factor is the gentle dip of the ruptured fault plane- which caused the along-dip directivity effect towards the footwall.

In addition, the main shock epicenter is located in the northern part of the area affected by landslides, which extends approximately 100 km to the south of the epicenter. The pattern suggests that the direction of rupture propagation was from north to south, which is also consistent with the southward increase in PGA values (Table 1; Figure 5). The spatial distribution of liquefaction-affected areas also shows that liquefaction occurrences are mostly located south of the epicenter. This is consistent with the suggested direction of rupture propagation. Liquefaction was also documented as far as 110 km south of the epicenter. It is well worth mentioning that the occurrences of landslide and liquefaction during the 2022 M_w 7.0 Northwestern Luzon Earthquake coincided with the DOST-PHIVOLCS regional scale earthquake-related hazard maps (PHIVOLCS, 2022f). The comparisons of the actual occurrences of earthquake-induced landslides and liquefactions with existing hazard maps are shown in Supplementary Figures S1, S2. Moreover, many rock falls and landslides occurred along road-cut slopes. This is because slope cutting increases the slope gradient, induces weathering, and degrades the rock mass quality.

The 2022 M_w 7.0 Northwestern Luzon Earthquake generated by the Abra River Fault was the first magnitude 7 earthquake along the segments of the Philippine Fault after the 1990 M_w 7.7 Luzon Earthquake. With a higher magnitude and an epicenter in a populated and developed area, the 1990 Luzon earthquake is considered to be the most destructive earthquake in the Philippines. It accounted for about 0.5 billion US dollars in property damage with 1,600 persons killed and geologic impacts including widespread landslides and liquefaction. The 1990 Luzon earthquake was caused by the movement of the Digdig Fault, a segment of the Philippine Fault that ruptured for about 120 km long (Nakata et al., 1996). Recent movements along the Philippine Fault also generated surface ruptures such as the 1973 M_w 7.0 Ragay Gulf Earthquake (Morante, 1974; Tsutsumi et al., 2015), the 2003 M_w 6.2 Masbate Earthquake (PHIVOLCS QRT, 2003), the 2017 M_w 6.5 Surigao Earthquake (PHIVOLCS QRT, 2018a), the 2017 M_w 6.5 Leyte Earthquake (PHIVOLCS QRT, 2018b) and the 2020 M_w 6.6 Masbate Earthquake (PHIVOLCS, 2020). Most of these recent surface rupturing earthquakes were magnitude 6 except for the 1973 Ragay Gulf Earthquake. Among these recent earthquakes along the Philippine Fault, the 2022 Northwestern Luzon Earthquake has no clear indication of a surface rupture based on field data and InSAR analysis.

The occurrence of the 2022 M_w 7.0 Northwestern Luzon Earthquake challenges our understanding of the characteristics of the Philippine Fault in northern Luzon and in general, the seismicity of the Philippines. The parameters derived from this earthquake are inconsistent with the known characteristics of the mapped faults in the region. Inaccurate evaluation of the fault geometry and faulting mechanisms yield large uncertainties in how we assess the seismic hazards and risk as well as understand the style of deformation in the region. This earthquake underscores the necessity to exert more effort to clarify the distribution, kinematics, geometry and mechanisms of faults through seismotectonic analysis.

In terms of structural and socio-economic impacts, this earthquake provides an opportunity to re-evaluate the earthquake preparedness and contingency planning effort of the national and local government units and the community. While uncertainties prevail in the seismic hazard assessment, the issue of preparedness becomes one of the most important measures. Damages to structures can be attributed to poor construction practices, improper building designs and substandard construction materials. Future efforts should focus on the design and construction of earthquake-resistant buildings and adherence to the National Building Code of the Philippines.

6 Summary and conclusion

This paper aims to serve as a quick and accessible reference for future researchers and other stakeholders about the 2022 M_w 7.0 Northwestern Luzon Earthquake. We present the results of the 11-day field investigations of the impacted area and the preliminary analysis of the causative fault. This earthquake greatly affected two provinces, Abra and Ilocos Sur, and was generated by one of the segments of the Philippine Fault, the Abra River Fault. Landslides and

tension cracks from this event persist as a significant threat to the community, as this remains to be unstable and can be triggered by aftershocks and heavy rains in the upcoming months.

Field investigation and InSAR analysis indicate no evidence of a surface rupture, however, the aftershock distribution, focal mechanism, deformation analysis, PGA values and the spatial distribution of mapped geologic impacts, such as landslides and liquefaction, provide further constraints on the characteristics of the causative fault. Additional analysis using geodetic and dislocation modeling may also provide support in characterizing this fault. This earthquake provided an opportunity to better understand the nature of faulting in the region. Information about the Abra River Fault needs to be reviewed and active tectonics and geophysical studies should be conducted in the future to better understand this fault, as well as the other segments of the Philippine Fault. The uncertainties in the seismic hazard assessment due to the lack of understanding of faulting in the region emphasize the importance of exerting efforts on earthquake preparedness and contingency planning.

Data availability statement

The original contributions presented in the study are included in the article/Supplementary Material, further inquiries can be directed to the corresponding author.

Author contributions

JP and DL: conceptualization and final integration of the manuscript; writing, editing and review of the manuscript; field investigation, data acquisition and analysis; map and figure preparation and finalization. KL and RC: field investigation, data acquisition and analysis; map and figure preparation and finalization; writing and review of the manuscript. MD, DB, CL, RD, MQ, RG, RP, CR, and MP: field investigation, data acquisition and analysis; map and figure preparation; writing and review of the manuscript.

Funding

The DOST-PHIVOLCS QRT field activities and this research was provided by the DOST-PHIVOLCS Internal Funds based on the Philippine government General Appropriations Act (GAA) of 2022.

Acknowledgments

The authors would like to acknowledge all the members of the DOST-PHIVOLCS QRT who participated in the field investigation and the DOST-PHIVOLCS for logistical and office support. We also would like to thank the assistance of the different government agencies and local government units of the affected areas. Special thanks to the Philippine Air Force Tactical Operations Group 1 for the aerial survey and to the Office of Civil Defense (OCD) and DOST Ilocos and Cordillera Autonomous Regions and the Abra and Ilocos Sur Provincial Science and Technolgy Centers (PSTC) for facilitating our field investigation. The Sentinel-1 SAR data are provided by the European Space Agency (ESA) and accessed through the Alaska Satellite Facility.

Conflict of interest

The authors declare that the research was conducted in the absence of any commercial or financial relationships that could be construed as a potential conflict of interest.

Publisher's note

Supplementary material

The Supplementary Material for this article can be found online at: https://www.frontiersin.org/articles/10.3389/feart.2023.1091595/full#supplementary-material

SUPPLEMENTARY TABLE S1
Location of geologic impacts during the 2022 Mw7.0 Northwestern Luzon Earthquake.

SUPPLEMENTARY FIGURE S1
Earthquake-induced landslide occurrences during the 2022 Mw7.0 Northwestern Luzon Earthquake and the DOST-PHIVOLCS Earthquake-Induced Landslide Hazard Map.

SUPPLEMENTARY FIGURE S2
Liquefaction occurrences during the 2022 Mw7.0 Northwestern Luzon Earthquake and the DOST-PHIVOLCS Earthquake-Induced Landslide Hazard Map.

References

Abrahamson, N. A., and Silva, W. J. (1997). Empirical response spectral attenuation relations for shallow crustal earthquakes. *Seismol. Res. Lett.* 68, 94–127. doi:10.1785/gssrl.68.1.94

Aurelio, M. A., Dianala, J. D. B., Taguibao, K. J. L., Pastoriza, L. R., Reyes, K., Sarande, R., et al. (2017). Seismotectonics of the 6 February 2012 Mw 6.7 Negros earthquake, central Philippines. *J. Asian Earth Sci.* 142, 93–108. doi:10.1016/j.jseaes.2016.12.018

Aurelio, M. A. (2000). Shear partitioning in the Philippines: Constraints from Philippine fault and global positioning system data. *Isl. Arc* 9 (4), 584–597. doi:10.1111/j.1440-1738.2000.00304.x

Barrier, E., Huchon, P., and Aurelio, M. (1991). Philippine Fault: A key for Philippine kinematics. *Geology* 19 (1), 32–35. doi:10.1130/00917613(1991)019<0032:PFAKFP>2.3.CO;2

Bautista, M. L. P., and Oike, K. (2000). Estimation of the magnitudes and epicenters of Philippine historical earthquakes. *Tectonophysics* 317 (1-2), 137–169. doi:10.1016/S0040-1951(99)00272-3

Bonita, J. D., Kumagai, H., and Nakano, M. (2015). Regional moment tensor analysis in the Philippines: CMT solutions in 2012–2013. *J. Disaster Res.* 10 (1), 18–24. doi:10.20965/jdr.2015.p0018

Chang, T. Y., Cotton, F., Tsai, Y. B., and Angelier, J. (2005). Quantification of hanging-wall effects on ground motion: Some insights from the 1999 Chi-Chi earthquake. *Bull. Seismol. Soc. Am.* 94 (94), 2186–2197. doi:10.1785/0120030233

Daligdig, J. A. (1997). *Recent faulting and paleoseismicity along the Philippine Fault Zone, North Central Luzon, Philippines*. D.Sc. Dissertation (unpublished), (Kyoto, Japan: Kyoto University), 73.

Donahue, J. L., and Abrahamson, N. A. (2014). Simulation-based hanging wall effects. *Earthq. Spectra* 30 (3), 1269–1284. doi:10.1193/071113EQS200M

Duquesnoy, T., Barrier, E., Kasser, M., Aurelio, M., Gaulon, R., Punongbayan, R. S., et al. (1994). Detection of creep along the Philippine Fault: First results of geodetic measurements on Leyte island, central Philippine. *Geophys. Res. Lett.* 21 (11), 975–978. doi:10.1029/94GL00640

Dziewonski, A. M., Chou, T. A., and Woodhouse, J. H. (1981). Determination of earthquake source parameters from waveform data for studies of global and regional seismicity. *J. Geophys. Res.* 86, 2825–2852. doi:10.1029/JB086iB04p02825

Ekström, G., Nettles, M., and Dziewonski, A. M. (2012). The global CMT project 2004-2010: Centroid-moment tensors for 13,017 earthquakes. *Phys. Earth Planet Interiors* 200-201, 1–9. doi:10.1016/j.pepi.2012.04.002

Fitch, T. J. (1972). Plate convergence, transcurrent faults, and internal deformation adjacent to Southeast Asia and the Western Pacific. *J. Geophys. Res.* 77 (23), 4432–4460. doi:10.1029/JB077i023p04432

Galgana, G., Hamburger, M., McCaffrey, R., Corpuz, E., and Chen, Q. Z. (2007). Analysis of crustal deformation in Luzon, Philippines using geodetic observations and earthquake focal mechanisms. *Tectonophysics* 432 (1-4), 63–87. doi:10.1016/j.tecto.2006.12.001

Geoscope Observatory (2022). Earthquake catalog. Avaialable at: http://geoscope.ipgp.fr/index.php/en/catalog/earthquake-description?seis=us6000i5rd (Accessed November 2, 2022).

GFZ German Research Centre for Geosciences (2022). GEOFON earthquake info. Avaialable at: https://geofon.gfz-potsdam.de/eqinfo/event.php?id=gfz2022oogo (Accessed November 2, 2022).

Global Centroid Moment Tensor (2022). Global CMT web page. Avaialable at: https://www.globalcmt.org/ (Accessed November 2, 2022).

Gorum, T. (2013). *Towards a better understanding of earthquake-triggered landslide: An analysis of the size, distribution pattern and characteristics of coseismic landslides in different tectonic and geomorphic environments*. Netherlands: D.Sc. Dissertation. University of Twente.

Lagmay, A. M. F., and Eco, R. (2014). Brief Communication: On the source characteristics and impacts of the magnitude 7.2 Bohol earthquake, Philippines. *Nat. Hazards Earth Syst. Sci.* 14, 2795–2801. doi:10.5194/nhess-14-2795-2014

Mines and Geosciences Bureau (MGB) (2008). *Geological maps of the Philippines*. Quezon City.

Morante, E. M. (1974). The Ragay Gulf earthquake of March 17, 1973, southern Luzon, Philippines. *J. Geol. Soc. Philipp.* 28 (2), 1–31.

Nakano, M., Kumagai, H., and Inoue, H. (2008). Waveform inversion in the frequency domain for the simultaneous determination of earthquake source mechanism and moment function. *Geophys. J. Int.* 173 (3), 1000–1011. doi:10.1111/j.1365-246X.2008.03783.x)

Nakata, T., Tsutsumi, H., Punongbayan, R. S., Rimando, R. E., Daligdig, J. A., Daag, A. S., et al. (1996). *Surface fault ruptures of the 1990 Luzon earthquake, Philippines, special publication 25*. Hiroshima, Japan: Research Center for Regional Geography, Hiroshima University, 86.

National Disaster Risk Reduction and Management Council (NDRRMC) (2022). Situational report No. 20 for magnitude 7.0 EQ in Tayum, Abra. Avaialable at: https://monitoring-dashboard.ndrrmc.gov.ph/assets/uploads/situations/SITREP_NO__20_FOR_MAG_7_0_EQ_IN_TAYUM_ABRA__2022_.pdf (Accessed October 10, 2022).

Papiona, K. L., and Kinugasa, Y. (2008). Trenching surveys along the Masbate segment of the Philippine fault zone. *J. Geol. Soc. Philipp.* 64, 19–53.

Perez, J. S., Tsutsumi, H., Cahulogan, M. T. C., Cabanlit, D. P., Abigania, M. I. T., and Nakata, T. (2015). Fault distribution, segmentation and earthquake generation potential of the Philippine fault in eastern Mindanao, Philippines. *J. Disaster Res.* 10 (1), 74–82. doi:10.20965/jdr.2015.p0074

Perez, J. S., and Tsutsumi, H. (2017). Tectonic geomorphology and paleoseismology of the Surigao segment of the Philippine fault in northeastern Mindanao Island, Philippines. *Tectonophysics* 699, 244–257. doi:10.1016/j.tecto.2017.02.001

Philippine Institute of Volcanology and Seismology (PHIVOLCS) (2013). The 15 October 2013 magnitude 7.2 Bohol earthquake. Available at: https://phivolcs.dost.gov.ph/index.php/earthquake/destructive-earthquake-of-the-philippines (Accessed October 10, 2022).

Philippine Institute of Volcanology and Seismology (PHIVOLCS) (2015). 06 February 2012 Ms 6.9 Negros Oriental earthquake. PHIVOLCS Special Report. Available at: https://www.phivolcs.dost.gov.ph/index.php/publications/special-report (Accessed October 10, 2022).

Philippine Institute of Volcanology and Seismology (PHIVOLCS) (2019). The 2019 series of earthquakes in Cotabato and vicinity. Available at: https://phivolcs.dost.gov.ph/index.php/earthquake/destructive-earthquake-of-the-philippines (Accessed October 10, 2022).

Philippine Institute of Volcanology and Seismology (PHIVOLCS) (2020). The 2020 magnitude 6.6 Masbate earthquake. Available at: https://www.phivolcs.dost.gov.ph/index.php/earthquake/destructive-earthquake-of-the-philippines.

Philippine Institute of Volcanology and Seismology (PHIVOLCS) (2022a). Distribution of active faults in the Philippines. Available at: https://www.phivolcs.dost.gov.ph/index.php/earthquake/earthquake-generators-of-the-philippines (Accessed October 10, 2022).

Philippine Institute of Volcanology and Seismology (PHIVOLCS) (2022b). Earthquake catalogue from 1907 to 2020.

Philippine Institute of Volcanology and Seismology (PHIVOLCS) (2022c). Earthquake information No.: 3. Available at: https://www.phivolcs.dost.gov.ph/2022_Earthquake_Information/July/2022_0727_0043_B3F.html (Accessed October 10, 2022).

Philippine Institute of Volcanology and Seismology (PHIVOLCS) (2022d). PHIVOLCS Earthquake Intensity Scale (PEIS). Available at: https://www.phivolcs.dost.gov.ph/index.php/earthquake/earthquake-intensity-scale (Accessed October 10, 2022).

Philippine Institute of Volcanology and Seismology (PHIVOLCS) (2022e). SWIFT earthquake source parameters. Available at: https://swift1.phivolcs.dost.gov.ph/~pvjica/events/20220727004328/20220727004328_v5.html (Accessed October 10, 2022).

Philippine Institute of Volcanology and Seismology (PHIVOLCS) (2022f). Earthquake-related hazards maps in the Philippines. Available at: https://phivolcs.dost.gov.ph/index.php/gisweb-hazard-maps (Accessed October 10, 2022).

PHIVOLCS Quick Response Team (2003). The 15 February 2003 masbate earthquake (special report No. 5). Available at: https://www.phivolcs.dost.gov.ph/index.php/earthquake/destructive-earthquake-of-the-philippines/17-earthquake/30-2003-february-15-ms6-2-masbate-earthquake (Accessed October 10, 2022).

PHIVOLCS Quick Response Team (2018a). 10 February 2017 Ms 6.7 Surigao del Norte Earthquake. PHIVOLCS Special Report 1 (1). Available at: https://www.phivolcs.dost.gov.ph/index.php/publications/special-report (Accessed October 10, 2022).

PHIVOLCS Quick Response Team (2018b). 06 July 2017 Ms 6.5 Leyte earthquake. PHIVOLCS Special Report 2 (1). Available at: https://www.phivolcs.dost.gov.ph/index.php/publications/special-report (Accessed October 10, 2022).

PHIVOLCS Quick Response Team (2019). 22 April 2019 magnitude 6.1 central Luzon earthquake PHIVOLCS Special Report 2 (1). Available at: https://www.phivolcs.dost.gov.ph/index.php/publications/special-report (Accessed October 10, 2022).

Pinet, N., and Stephan, J. F. (1990). The philippine wrench Fault System in the Ilocos foothills, northwestern Luzon, Philippines. *Tectonophysics* 183 (1-4), 207–224. doi:10.1016/0040-1951(90)90417-7

Punongbayan, B. J. T., Kumagai, H., Pulido, N., Bonita, J. D., Nakano, M., Yamashina, T., et al. (2015). Development and operation of a regional moment tensor analysis system in the Philippines: Contributions to the understanding of recent damaging earthquakes. *J. Disaster Res.* 10 (1), 25–34. doi:10.20965/jdr.2015.p0025

Rimando, J. M., Aurelio, M. A., Dianala, J. D. B., Taguibao, K. J. L., Agustin, K. M. C., Berador, A. E. G., et al. (2019). Coseismic ground rupture of the 15 October 2013 magnitude (Mw) 7.2 Bohol Earthquake, Bohol Island, Central Philippines. *Tectonics* 38, 2558–2580. doi:10.1029/2019TC005503

Rimando, J. M., Williamson, A. L., Mendoza, R. B. C., and Hobbs, T. E. (2022). Source model and characteristics of the 27 July 2022 Mw 7.0 northwestern Luzon earthquake, Philippines. *Seismica* 1 (1). doi:10.26443/seismica.v1i1.217

Rimando, R., and Knuepfer, P. (2006). Neotectonics of the Marikina Val-ley fault system (MVFS) and tectonic framework of structures in northern and central Luzon, Philippines. *Tectonophysics* 415 (1-4), 17–38. doi:10.1016/j.tecto.2005.11.009

Rimando, R., and Rimando, J. (2020). Morphotectonic kinematic indicators along the Vigan-Aggao Fault: The Western deformation front of the Philippine Fault zone in northern Luzon, the Philippines. *Geosciences* 10 (2), 83. doi:10.3390/geosciences10020083

Rimando, R. E., Rimando, J. M., and Lim, R. B. (2020). Complex shear partitioning involving the 6 February 2012 Mw 6.7 Negros Earthquake ground rupture in central Philippines. *Geoscience* 10 (11), 460. doi:10.3390/geosciences10110460

Ringenbach, J. C., Pinet, N., Stephan, J. F., and Delteil, J. (1993). Structural variety and tectonic evolution of strike-slip basins related to the Philippine Fault system, northern Luzon, Philippines. *Tectonics* 12 (1), 187–203. doi:10.1029/92TC01968

Ringenbach, J. C., Stephan, J. F., Maleterre, P., and Bellon, H. (1990). Structure and geological history of the Lepanto-Cervantes releasing bend on the Abra River Fault, Luzon Central Cordillera, Philippines. *Tectonophysics* 183, 224–241. doi:10.1016/0040-1951(90)90418-8

Rosen, P. A., Gurrola, E., Sacco, G. F., and Zebker, H. (2012). "The InSAR scientific computing environment". in, 9th European Conference on Synthetic Aperture Radar, EUSAR, 730–733.

Southeast Asia Association of Seismology and Earthquake Engineering (SEASSE) (1985). in Series of Seismology (Philippines) *IV*, 843.*Catalogue of philippine earthquakes*

Su, Z., Yang, Y. H., Li, Y. S., Xu, X. W., Zhang, J., Shou, X., et al. (2019). Coseismic displacement of the 5 april 2017 mashhad earthquake (Mw 6.1) in NE Iran through sentinel-1A TOPS data: New implications for the strain partitioning in the southern binalud mountains. *J. Asian Earth Sci.* 169, 244–256. doi:10.1016/j.jseaes.2018.08.010

Tsutsumi, H., Daligdig, J. A., Goto, H., Tungol, N. M., Kondo, H., Nakata, T., et al. (2006). *Timing of surface-rupturing earthquakes on the Philippine fault zone in central Luzon island, Philippines*. EOS Transactions, American Geophysical Union, 52.

Tsutsumi, H., and Perez, J. S. (2013). Large-scale digital mapping of the Philippine fault zone based on aerial photograph interpretation. *Act. Faults Res.* 39, 29–37. doi:10.11462/afr.2013.39_29

Tsutsumi, H., Perez, J. S., Marjes, J. U., Papiona, K. L., and Ramos, N. T. (2015). Coseismic displacement and recurrence interval of the 1973 Ragay Gulf earthquake, southern Luzon, Philippines. *J. Disaster Res.* 10 (1), 83–90. doi:10.20965/jdr.2015.p0083

U.S. Geological Survey (2022). Earthquake event page. Avaialable at: https://earthquake.usgs.gov/earthquakes/eventpage/us6000i5rd/executive (Accessed November 2, 2022).

Xu, C., Xu, X., Shyu, J. B. H., Zheng, W., and Min, W. (2014). Landslides triggered by the 22 July 2013 Minxian–Zhangxian, China, Mw 5.9 earthquake: Inventory compiling and spatial distribution analysis. *J. Asian Earth Sci.* 92, 125–142. doi:10.1016/j.jseaes.2014.06.014

Yumul, G. P., Dimalanta, C. B., Marquez, E. J., and Maglambayan, V. B. (2008). Tectonic setting of a composite terrane: A review of the Philippine island arc system. *Geosci. J.* 12 (1), 7–17. doi:10.1007/s12303-008-0002-0

Zang, S. X., Chen, Q. Y., Ning, J. Y., Zheng, K. S., and Yong, G. L. (2002). Motion of the Philippine Sea plate consistent with the NUVEL-1A model. *Geophys. J. Int.* 150 (3), 809–819. doi:10.1046/j.1365-246X.2002.01744.x